Quantifying the Coverage Density of Poly(ethylene glycol) Chains on the Surface of Gold Nanostructures

Xiaohu Xia[†,‖,§], **Miaoxin Yang**[†,§], **Yucai Wang**[†], **Yiqun Zheng**[⊥], **Qingge Li**[‖], **Jingyi Chen**[†,‡,*], and **Younan Xia**[†,€,*]

[†]Department of Biomedical Engineering, Washington University, St. Louis, Missouri 63130, United States

[‡]Department of Chemistry and Biochemistry, University of Arkansas, Fayetteville, Arkansas 72701, United States

[‖]Engineering Research Center of Molecular Diagnostics, School of Life Sciences, Xiamen University, Xiamen, Fujian 361005, P. R. China

[⊥]Department of Chemistry, Washington University, St. Louis, Missouri 63130, United States

Abstract

The coverage density of poly(ethylene glycol) (PEG) is a key parameter in determining the efficiency of PEGylation, a process pivotal to *in vivo* delivery and targeting of nanomaterials. Here we report four complementary methods for quantifying the coverage density of PEG chains on various types of Au nanostructures by using a model system based on HS-PEG-NH$_2$ with different molecular weights. Specifically, the methods involve reactions with fluorescamine and ninhydrin, as well as labeling with fluorescein isothiocyanate (FITC) and Cu^{2+} ions. The first two methods use conventional amine assays to measure the number of unreacted HS-PEG-NH$_2$ molecules left behind in the solution after incubation with the Au nanostructures. The other two methods involve coupling between the terminal –NH$_2$ groups of adsorbed -S-PEG-NH$_2$ chains and FITC or a ligand for Cu^{2+} ion, and thus pertain to the "active" –NH$_2$ groups on the surface of a Au nanostructure. We found that the coverage density decreased as the length of PEG chains increased. A stronger binding affinity of the initial capping ligand to the Au surface tended to reduce the PEGylation efficiency by slowing down the ligand exchange process. For the Au nanostructures and capping ligands we have tested, the PEGylation efficiency decreased in the order of citrate-capped nanoparticles > PVP-capped nanocages ≈ CTAC-capped nanoparticles ≫ CTAB-capped nanorods, where PVP, CTAC, and CTAB stand for poly(vinyl pyrrolidone), cetyltrimethylammonium chloride, and cetyltrimethylammonium bromide, respectively.

[*]Address correspondence to younan.xia@bme.gatech.edu, chenj@uark.edu.
[§]These two authors contributed equally to this work.
[€]Current address: The Wallace H. Coulter Department of Biomedical Engineering, Georgia Institute of Technology and Emory University Medical School, School of Chemistry and Biochemistry, Georgia Institute of Technology, Atlanta, Georgia 30332, United States

Supporting Information Available: UV-vis spectra of the 50-nm AuNCs before and after functionalization with HS-PEG$_{3000}$-NH$_2$ or HS-PEG$_{3000}$-COOH at 4 °C and 22 °C; scheme of the reaction involving a primary amine and fluresceamine (or ninhydrin); typical excitation and emission spectra of the chromophore derived from fluorescamine and HS-PEG-NH$_2$; fluorescence and UV-vis spectra of HS-PEG$_{5000}$-NH$_2$ standard solutions; calibration curve obtained for HS-PEG$_{5000}$-NH$_2$ at pH = 6.5 using the fluorescamine-based assay; calibration curve for free FITC; calculations of surface areas for different types of Au nanostructures; and a table of characterization of AuNCs with different surface coatings under different temperatures. This material is available free of charge *via* the Internet at http://pubs.acs.org.

Keywords

Au nanostructure; PEGylation; ligand exchnage; capping ligand

Inorganic nanomaterials have attracted widespread interest as a multifunctional platform for various applications in biology and medicine.[1–3] Among them, Au nanostructures have been used as both imaging and therapeutic agents for diagnosis and treatment of diseases such as cancer.[4–10] To be useful *in vivo*, it is critical to have the nanoparticles delivered to the site of interest without being accumulated in healthy tissues and organs. The nanoparticles, therefore, must have the ability to bypass the reticuloendothelial system (RES), circulate in the bloodstream for a long period of time, and preferentially accumulate at the site of interest. Poly(ethylene glycol) (PEG) is the most widely used polymer for masking nanoparticles from clearance by RES due to its ability to resist protein adsorption, excellent biocompatibility, and commercial availability.[11–14] The success of PEGylation critically depends on the coverage density of PEG chains on the surface of a nanoparticle, herein referred to as the number of PEG chains per nm^2 of the particle surface. Essentially, the coverage density of PEG chains represents one of the key parameters in determining the efficiency of PEGylation and thereby the protein repelling capability of resultant nanoparticles and their circulation half-life.[15,16]

PEGylation of Au nanostructures is typically achieved through a ligand exchange process by using thiol-terminated PEG molecules.[17–19] For chemically synthesized Au nanostructures, they are often covered and stabilized by different capping ligands depending on the protocols. During PEGylation, the capping ligands are displaced by -S-PEG chains due to a stronger Au-S linkage and an energy gain associated with the intermolecular interaction.[20] Different methods have been employed to assess the efficiency of PEGylation, including those that directly measure changes to the physical properties of nanoparticles such as solubility, stability, hydrodynamic diameter, and zeta potential. None of these methods, however, can provide quantitative information with regard to the number of PEG chains on the surface of a particle. Thermal gravity analysis (TGA) has been widely used to estimate the number of PEG chains on the surface of a nanoparticle.[21] It measures the mass difference before and after removal of PEG chains due to thermal desorption and decomposition. To measure the mass change accurately, it requires the use of a relatively large quantity of the sample. The coverage density calculated from TGA data corresponds to the total number of PEG chains in the sample, including those loosely trapped among the particles. When the other end of a PEG chain is terminated in a different functional group like $–NH_2$, not all the terminal groups can be activated and coupled to another ligand such as a targeting moiety. In this case, there is also a critical need to quantify both the total and "active" $–PEG-NH_2$ chains on the surface of a Au nanoparticle. Here we accomplish this goal by using a combination of four complementary methods.

We focused on $HS-PEG-NH_2$ molecules with different molecular weights because $–NH_2$ is one of the most commonly used functional group for further conjugation through amide coupling with the carboxylate or carboxylic acid group.[22,23] Various reagents such as fluorescamine and ninhydrin have been used to quantitatively analyze the number of primary amines in small molecules, peptides, and proteins.[24–26] The fluorescamine-based assay involves the production of a fluorescent compound that can be quantified by fluorescence spectroscopy with high sensitivity while the ninhydrin-based assay yields a chromophore with strong absorption in the visible that can be measured using ultraviolet-visible (UV-vis) spectroscopy. In this article, we apply these two assays to quantify the total number of $HS-PEG-NH_2$ molecules left behind in the reaction solution after incubation with various types of Au nanostructures. We determined the coverage density of $–S-PEG-NH_2$

chains on the surface of a Au nanostructure and systematically studied the adsorption kinetics of HS-PEG-NH$_2$ with different molecular weights. We also compared the PEGylation efficiencies for Au nanostructures with different morphologies and/or initially capped by different types of ligands. At the same time, we developed two new methods for quantitatively measuring the number of "active" –S-PEG-NH$_2$ chains on the surface of a Au nanostructure using assays based on dye- and Cu^{2+}-labeling. This study provides a set of useful guidelines for the PEGylation of Au nanostructures towards a range of biomedical applications.

Results and Discussion

We used four different methods to measure the coverage density of –S-PEG-NH$_2$ chains on the surface of a Au nanostructure, including fluorescence assays based on fluorescamine and fluorescein isothiocyanate (FITC)-labeling, UV-vis spectroscopy assay involving ninhydin, and inductively coupled plasma mass spectrometry (ICP-MS) analysis based on Cu^{2+}-labeling. Figure 1 schematically illustrates the principles of these four methods. Both the fluorescamineand ninhydrin-based assays measure the concentration of unreacted HS-PEG-NH$_2$ molecules left behind in the supernatant of a sample using fluorescence and UV-vis absorption, respectively. These two methods yield the total number of –S-PEG-NH$_2$ chains on the entire surface of all Au nanostructures in the sample after the amount of HS-PEG-NH$_2$ remaining in the supernatant has been subtracted from the amount of HS-PEG-NH$_2$ added to the original solution. For the other two methods, the Au-S-PEG-NH$_2$ conjugates are labeled with FITC molecules or Cu^{2+} ions and precipitated out from the solution for fluorescence and ICP-MS measurements, respectively, after the Au nanostructures have been selectively dissolved with an etching solution. The outputs of these two methods are the coverage densities of "active" –S-PEG-NH$_2$ chains on the surface of a Au nanostructure that could be labeled with FITC or Cu^{2+}.

Synthesis of Au Nanostructures and PEGylation of Their Surfaces *via* Ligand Exchange

Gold nanostructures were prepared with four different capping ligands: poly(vinyl pyrrolidone) (PVP), cetyltrimethylammonium chloride (CTAC), cetyltrimethylammonium bromide (CTAB), and citrate ions. Their surfaces were then modified with HS-PEG-NH$_2$ using a ligand exchange process. Figure 2 shows TEM images of PVP-capped Au nanocages (AuNCs) with edge lengths of 30, 50, and 60 nm, respectively; CTAC-capped Au nanoparticles (AuNPs) with an avarage diameter of 40 nm; citrate-capped AuNPs with an avarage diameter of 42 nm; and CTAB-capped Au nanorods (AuNRs) with avarage dimensions of 80 nm × 22 nm.

During ligand exchange, HS-PEG-NH$_2$ could displace the original capping ligand on the surface of a Au nanostructure thanks to a relatively strong Au-S bond and the energy gained through intermolecular interactions between the PEG chains. Interestingly, the outcome of a ligand exchange process was found to have a strong dependence on the reaction temperature for PEG chains with relatively low molecular weights (*e.g.*, PEG$_{3000}$ and PEG$_{5000}$). The localized surface plasmon resonance (LSPR) peak of the AuNCs only showed very minor red-shifts after incubation with HS-PEG-NH$_2$ in three different molecular weights at 4 °C (Fig. 3A), which can be ascribed to the slight changes in reflective index at the interface. The LSPR peak was essentially retained in shape and width, implying that the AuNCs remained to be well dispersed in the medium after ligand exchange and no aggregation had occurred. When conducted at 22 °C, however, the LSPR peak of the AuNCs was significantly broadened after surface modification with PEG chains of 3,000 and 5,000 in molecular weight (Fig. 3B), indicating that aggregation had occurred in the system. When PEG of 20,000 in molecular weight was used, no aggregation was observed. In addition, the PVP-covered AuNCs showed no change to its UV-vis spectrum when the sample was aged

at 4 °C and 22 °C (Fig. S1). We observed no change to the spectrum either when the PVP-covered AuNCs were conjugated with HS-PEG-COOH at 4 °C while the peak intensity was slightly reduced when the conjugation was conducted at 22 °C. These results were consistent with the particle sizes and zeta potentials measured by dynamic light scattering (DLS) (Table S1). The aggregation observed for both samples involving HS-PEG$_{3000}$-NH$_2$ and HS-PEG$_{5000}$-NH$_2$ at 22 °C can be attributed to the direct connection of two AuNCs by HS-PEG-NH$_2$ and/or to the presence of some thiol groups on the outmost surface of AuNCs, which are susceptible to cross-linking *via* the formation of a disulfide (S-S) bond between two AuNCs. At 22 °C, both the –NH$_2$ and –SH groups of a HS-PEG-NH$_2$ molecule could interact with a Au surface to generate Au-S and Au-N bonds with energies in the range of 30–40 kcal/mol[27] and 5–10 kcal/mol,[28,29] respectively. At 4 °C, however, the Au-S bond was preferentially formed over the Au-N bond probably due to a kinetic reason, leading to the presence of fewer –SH groups on the outer surface. Such a dependence of selectivity on temperature was also observed by other groups for thiol molecules terminated in the amino group.[30] As a result, we observed a more positively charged surface and less significant aggregation for the AuNCs conjugated with HS-PEG-NH$_2$ of the same molecular weight at 4 °C than those at 22 °C. This phenomenon, however, was not observed for PEG of 20,000 in molecular weight probably due to its randomly-coiled conformation.[31,32]

Quantification Using the Fluorescamine-Based Assay

The fluorescamine-based assay was originally developed for quantification of primary amines in biomolecules with sensitivity on the pM scale.[24] In this assay, non-fluorescent fluorescamine reacts with a primary amine to generate a fluorescent product that emits light at 480 nm when excited at 390 nm (Figs. S2 and S3 in the Supporting Information). Figure 4A shows a calibration curve that correlates the fluorescence intensity at 480 nm with the concentration of HS-PEG-NH$_2$. The assay was performed under a basic condition (pH 10) and the typical fluorescence spectra are shown in Figure S4A. Similar to primary aliphatic amine, the pKa of the amine terminus in HS-PEG-NH$_2$ is in the range of 9–11.[33] At an acidic pH (*e.g.*, 6.5), the protonated amine could not react with fluorescamine effectively, resulting in a poor linearity for the calibration curve (Fig. S5). In a basic solution, the primary amine was deprotonated and thus became highly reactive toward fluorescamine. Linear relationships were found up to µM concentrations with the slopes decreasing in the order of HS-PEG$_{3000}$-NH$_2$ > HS-PEG$_{5000}$-NH$_2$ > HS-PEG$_{20000}$-NH$_2$. This trend suggests that the amine terminus of PEGs with low molecular weights reacted with fluorescamine more efficiently than those with high molecular weights. Previous studies showed that a helical conformation was preferred by PEG due to the formation of hydrogen bonds between the neighboring oxygen atoms and water molecules.[34,35] As such, all the amino groups will be completely exposed at the surface. When the molecular weight of PEG is increased beyond a certain number, however, the helical structure will become less favored. The random coil conformation taken by the polymer chains tends to engulf the amino groups, reducing their accessibility and reactivity.[36,37]

We then applied the assay to measure the coverage density of HS-PEG-NH$_2$ chains on the surface of Au nanostructures. Figure 4B shows fluorescence spectra taken from the original HS-PEG-NH$_2$ solutions and the supernatants after incubation with the 50-nm AuNCs. The decrease in fluorescence intensity corresponds to the amount of HS-PEG-NH$_2$ that had been conjugated to the surface of AuNCs. By comparing the fluorescent intensities with the calibration curves, the average numbers of HS-PEG-NH$_2$ molecules attached to the surface of one 50-nm AuNC were estimated to be 24,700±1,200, 12,700±3,340 and 2,100±740 for –S-PEG$_{3000}$-NH$_2$, –S-PEG$_{5000}$-NH$_2$, and –S-PEG$_{20000}$-NH$_2$, respectively. Herein, the surface area of a AuNC is defined as the outer surface area of a AuNC with the inner surface and pores being excluded since the outer surface is more accessible than the inner surface due to

a relatively small pore size for the AuNC (ca. 5 nm in diameter for the 50-nm AuNC). Accordingly, the surface area of a 50-nm AuNC was estimated to be 15,000 nm^2. As such, the footprint of an individual $-S-PEG-NH_2$ chain on the surface of 50-nm AuNC could be derived as 0.61, 1.18, and 7.14 nm^2, for $-S-PEG_{3000}-NH_2$, $-S-PEG_{5000}-NH_2$ and $-S-PEG_{20000}-NH_2$, respectively. Accordingly, the coverage densities of PEG chains were 1.64, 0.85, and 0.14 per nm^2 for $-S-PEG_{3000}-NH_2$, $-S-PEG_{5000}-NH_2$, and $-SPEG_{20000}-NH_2$, respectively.

Quantification Using the Ninhydrin-Based Assay

In the ninhydrin-based assay, ninhydrin reacts with the primary amine to generate a chromophore in deep blue or purple color, known as Ruhemann's purple (Fig. S6).[25] In a typical reaction, the color was developed over a short period of time depending on the reactivity of the amine group and could reach a maximum intensity in 4 min.[26] Figure 5A shows the calibration curves for HS-PEG-NH_2 that correlate the absorbance at 565 nm with the concentration of HS-PEG-NH_2. Similar to the fluorescamine-based assay, linear relationships were found up to µM concentrations with the slopes decreasing in the order of $HSPEG_{3000}-NH_2$ > HS-$PEG_{5000}-NH_2$ > HS-$PEG_{20000}-NH_2$. In general, the detection sensitivity of ninhydrin-based assay was much lower than that of fluorescamine-based assay. For example, HS-$PEG_{5000}-NH_2$ could still be detected at a concentration of 250 nM by the fluorescamine-based assay (Fig. S4A) while it became very difficult to measure using the ninhydrin-based assay at a concentration of 500 nM (Fig. S4B). Figure 5B shows the UV-vis spectra taken from the original HS-PEG-NH_2 solution and from the supernatants after incubation with 50-nm AuNCs. The drop in absorbance was directly proportional to the number of HS-PEG-NH_2 molecules that had been attached to the surface of AuNCs. The average numbers of $-S-PEG-NH_2$ per AuNC were found to be 33,170±2,750, 20,000±2,400, and 3,200 ±1,770 for $-S-PEG_{3000}-NH_2$, $-SPEG_{5000}-NH_2$, and $-S-PEG_{20000}-NH_2$, respectively. The coverage densities of PEG chains were 2.21, 1.33, and 0.21 per nm_2 for $-S-PEG_{3000}-NH_2$, $-S-PEG_{5000}-NH_2$, and $-S-PEG_{20000}-NH_2$, respectively.

Both fluorescamine- and ninhydrin-based assays gave the number of unreacted HS-PEG-NH_2 molecules in the solution, which could then be converted to the number of -S-PEG-NH_2 chains on the surface of AuNCs. As shown in Table 1, the ninhydrin-based assay was found to consistently give a larger number of PEG chains per AuNC as compared to the fluorescamine-based assay. The discrepancy between these two assays could be attributed to a phenomenon known as metal-enhanced fluorescence (MEF).[38,39] Although both assays measured the number of unreacted HS-PEG-NH_2 molecules in the supernatant, any small amount of AuNCs left in the supernatant might enhance the fluorescence intensity while causing no change to the absorbance because there was no overlap between the absorption peaks of AuNCs and the dye. As a result, the fluorescamine-based assay tended to produce a smaller difference for the samples before and after PEGylation, and thus giving a smaller number of PEG chains on each AuNC in comparison with the ninhydrin-based assay. In general, the ninhydrin-based assay is less sensitive to sample preparation procedure (*e.g.*, complete sedimentation of all AuNCs or not) and should be more reliable for quantifying the number of $-S-PEG-NH_2$ chains. As a compromise, the ninhydrin-based assay has a much lower detection sensitivity compared to the fluorescamine-based assay. Depending on the physical properties of the sample, one needs to carefully choose a proper quantification method.

Quantification Using an Assay Based on FITC-Labeling

In this assay, FITC molecules were added and coupled to the $-NH_2$ groups on Au-S-PEG-NH_2 conjugates through a reaction involving isothiocyanate and amino groups. After conjugation, the fluorescence from FITC attached to the surface of Au nanostructures is

typically quenched due to a strong interaction between the electrons on the metal surface and the dipole of the dye, a phenomenon known as nano-surface energy transfer (NSET).[40,41] To recover the fluorescence, an aqueous KCN solution was added to completely dissolve the Au nanostructures, releasing the –S-PEG-FITC chains from the metal surface, probably in the form of disulfide. The intensity of fluorescence from the released -S-PEG-FITC is directly proportional to the number of "active" –NH_2 groups that could react with FITC. Figure 6 shows fluorescence spectra recorded from the –S-PEG-FITC molecules in three different lengths that had been released from the surface of 50-nm AuNCs. By comparing with a calibration curve (Fig. S7), the average numbers of "active" –NH_2 groups were found to be 8,860±990, 4,760±870 and 1,010±620 for –S-PEG_{3000}-NH_2, –S-PEG_{5000}-NH_2, and – S-PEG_{20000}-NH_2, respectively. The percentages of "active" –NH_2 groups for FITC conjugation versus the total –S-PEG-NH_2 chains measured using the fluorescamine-based assay were 35.9%, 37.5%, and 48.1% for –S-PEG_{3000}-NH_2, –S-PEG_{5000}-NH_2, and –S-PEG_{20000}-NH_2, respectively.

Quantification Using an Assay Based on Cu^{2+}-Labeling

In this method, the –NH_2 groups on the surface of Au-S-PEG-NH_2 conjugates were initially coupled with DOTA-NHS through an amide coupling reaction *via* NHS-activated ester, followed by loading of Cu^{2+} ions.[42–44] The resultant Au-S-PEG-DOTA-Cu^{2+} conjugates were then digested using aqua regia for ICP-MS measurement. The numbers of "active" –NH_2 groups on each AuNC were then derived from the numbers of loaded Cu^{2+} ions, which were found to be 7,000±3,200, 3,800±2,100 and 760±400 for –S-PEG_{3000}-NH_2, –S-PEG_{5000}-NH_2, and –S-PEG_{20000}-NH_2, respectively, per 50-nm AuNC. The percentages of "active" –NH_2 groups for DOTA conjugation and Cu^{2+} loading relative to the number of –S-PEG-NH_2 chains measured by the fluorescamine-based assay was 28.3%, 29.9%, and 36.2% for –S-PEG_{3000}-NH_2, –S-PEG_{5000}-NH_2, and –S-PEG_{20000}-NH_2, respectively. This trend was similar to what was obtained using an assay based on FITC-labeling. However, the number of active PEG-NH_2 units per 50-nm AuNC measured using the Cu^{2+}-labeling assay was lower than what was obtained using the FITC-labeling method. The discrepancy can be attributed to the difference in conjugation procedure: the FITC-labeling assay involved one-step conjugation while the Cu^{2+}-labeling assay required the use of two steps. In general, the coupling efficiency of a two-step process is always lower than that of a one-step process.

Characterization of the AuNC-S-PEG-NH_2 Conjugates

The hydrodynamic diameter and zeta potential of the AuNCs were expected to change as PVP was replaced by –S-PEG-NH_2 (Table 1). We used DLS to measure the hydrodynamic diameters and zeta potentials of the nanoparticles. After PEGylation, the AuNCs showed an increase in hydrodynamic diameter, suggesting that –S-PEG-NH_2 chains had been attached to the surface of AuNCs. In comparison with AuNC-S-PEG_{3000}-NH_2, the hydrodynamic diameter of AuNC-S-PEG_{5000}-NH_2 was increased by 22.6 nm due to the increased molecular weight for PEG. These two PEGs can both self-assemble as a brush-like structure on the surface of AuNC, and thus the hydrodynamic diameter is mainly determined by the PEG chain length.[45] For –S-PEG_{20000}-NH_2, however, the polymer chain tended to coil and take a mushroom-like conformation on the surface of AuNC.[31,32] As a result, the hydrodynamic diameter of AuNC-S-PEG_{20000}-NH_2 was smaller than that of AuNC-S-PEG_{5000}-NH_2. The surface modification by –S-PEG-NH_2 was also confirmed by the changes to surface charge before and after conjugation through zeta potential measurements. After PEGylation, the AuNCs showed an increase in zeta potential, which could be ascribed to the presence of positively charged –NH_2 group on the AuNC-S-PEG-NH_2 conjugates at pH ≈ 6.7 (deionized water). The zeta potentials decreased in the order of AuNC-S-PEG_{3000}-NH_2 (highly positive) > AuNC-S-PEG_{5000}-NH_2 (positive) ≫ AuNC-S-PEG_{20000}-NH_2

(slightly negative) > PVP-capped AuNC (negative). This trend is in agreement with the hydrodynamic diameter measurement and could provide some indirect information about the coverage density of –S-PEG-NH$_2$ chains on AuNCs, as well as the polymer chain conformation.

Adsorption Kinetics of HS-PEG-NH$_2$

We also studied the adsorption kinetics of HS-PEG-NH$_2$ for the functionalization of different types of Au nanostructures. The adsorption of a HS-containing aliphatic molecule onto a Au surface occurs very quickly, typically in few minutes, at room temperature.[20,46] To monitor the adsorption kinetics, the conjugation of Au nanostructures with HS-PEG-NH$_2$ was performed at 0 °C in an ice bath. The fluorescamine-based assay was chosen to quantify the coverage density of –S-PEG-NH$_2$ chains at different reaction times (*t*) due to its high sensitivity. Figure 7 compares the adsorption kinetics for HS-PEG$_{5000}$-NH$_2$ and Au nanostructures covered with different capping ligands. For PVP-capped AuNCs, fast kinetics was involved at the initial stage, by which 50% of the –S-PEG-NH$_2$ chains had been adsorbed onto the surface of AuNCs at $t \approx$ 10–15 min. After 20 min, the –S-PEG-NH$_2$ chains seemed to undergo a reorganization process through desorption and adsorption and finally the coverage density of PEG-NH$_2$ chains reached a plateau at $t \approx$ 100 min. The CTAC-capped AuNPs showed kinetics similar to what was observed for the PVP-capped AuNCs. For citrate-capped AuNPs, at $t \approx$ 5–10 min, 50% of –S-PEG-NH$_2$ chains were found to be adsorbed onto the surface of AuNPs, which was faster than the above two cases. An equilibrium state was reached at $t \approx$ 60 min. In the case of CTAB-capped AuNRs, however, much longer periods of time were required to reach both 50% coverage (at $t \approx$ 20–30 min) and an equilibrium state (at $t \approx$ 150 min).

The Effects of Particle Size and Capping Ligand on PEGylation

We investigated the effect of particle size on the efficiency of PEGylation by employing AuNCs with different edge lengths. For this purpose, 30-, 50- and 60-nm AuNCs (Fig. 2, A–C) were conjugated with HS-PEG$_{5000}$-NH$_2$ using the standard procedure at 4 °C. The average numbers of –S-PEG$_{5000}$-NH$_2$ chains per AuNC were found to be 3,300±1,040, 12,700±3,340 and 29,500±8,980, respectively, using the fluoresceamine-based assay. The coverage densities of –S-PEG$_{5000}$-NH$_2$ chains on the 30-, 50-, and 60-nm AuNCs were calculated as 0.61, 0.85, and 1.36 per nm^2, respectively. As the AuNCs became smaller, the areas of both corners and edges would increase relative to the side faces.[47] Due to the presence of curvature at the corner or edge site, the PEG chains would not be able to interact strongly or pack densely, so it is not unreasonable to expect the coverage density of PEG chains to drop as the particle size was reduced.

The initial capping ligand on the surface of Au nanostructures is also expected to play an important role in controlling the kinetics of ligand exchange with HS-PEG-NH$_2$ molecules. To study the effect of capping ligand on PEGylation, Au nanostructures with similar surface areas but capped with different ligands were reacted with HS-PEG$_{5000}$-NH$_2$ under the same reaction condition. The Au nanostructures we have examined include PVP-capped AuNCs of 30 nm in edge length, CTAC-capped AuNPs of 40 nm in diameter, citrate-capped AuNPs of 42 nm in diameter, and CTAB-capped AuNRs of 80 nm × 22 nm in dimensions (see Fig. 2). They had a similar surface area around 5,500 nm^2 (Fig. S8). After incubation with HS-PEG$_{5000}$-NH$_2$, the coverage densities of total -S-PEG-NH$_2$ chains and "active" –NH$_2$ groups on the surface of these Au NPs were determined using assays based on fluoresceamine and FITC-labeling, respectively. As shown in Table 2, the coverage densities of -S-PEG-NH$_2$ chains on the Au nanostructures decreased in the order of citrate-capped AuNPs > PVP-capped AuNCs ≈ CTAC-capped AuNPs ≫ CTAB-capped AuNRs. This trend implies that the displacement by –S-PEG-NH$_2$ chains was strongly dependent on

the binding affinity of the original capping ligand to the surface of a Au nanostructure, which decreased in the order of CTAB $\gg$ PVP $\approx$ CTAC > citrate. We believe that the presence of a compact bilayer of CTAB on the surface of AuNRs was responsible for the low coverage density of -S-PEG-NH$_2$ chains on the surface of CTAB-capped AuNRs after ligand exchange.[48–50] The coverage densities of "active" -NH$_2$ groups on these Au nanostructures were found to follow a similar trend in the order of citrate-capped AuNPs > PVP-capped AuNCs $\approx$ CTAC-capped AuNPs $\gg$ CTAB-capped AuNRs. The percentage of "active" –NH$_2$ groups *versus* total –S-PEG-NH$_2$ chains on the AuNCs was ~30% as compared to a value of ~50% for all three other types of Au NPs. These results imply a low coupling efficiency between FITC and the amino groups on the AuNCs, which is possibly due to the fact that some of the –S-PEG-NH$_2$ chains diffused through the pores and thus trapped inside the AuNCs. These –S-PEG-NH$_2$ molecules might be poorly accessible to the dye molecules. On the other hand, as compared to AuNPs with large curvature on the surface, the relatively flat surface of AuNCs could increase the packing density of PEG chains and thus reduce the accessibility and reactivity of terminal amino groups on the PEG chains.

Conclusions

In summary, we have demonstrated four complementary methods for quantitative analysis of the PEGylation efficiency of Au nanostructures, including the coverage density of -S-PEG-NH$_2$ chains and the "active" –NH$_2$ groups, by using assays based on reactions with fluoresceamine or ninhydrin, as well as labeling with a dye or Cu^{2+}. For a model system based on HS-PEG-NH$_2$ with different molecular weights and AuNCs with 50 nm in edge length, we found that: *i*) the number of -S-PEG-NH$_2$ chains per AuNC decreased in the order of –S-PEG$_{3000}$-NH$_2$ > –S-PEG$_{5000}$-NH$_2$ $\gg$ –S-PEG$_{20000}$-NH$_2$; and *ii*) the percentage of "active" –NH$_2$ groups versus the number of –S-PEG-NH$_2$ chains decreased in the same order. While the fluoresceamine-based assay was much more sensitive than the ninhydrin-based assay, the latter was less sensitive to the experimental details and thus most reliable among all four methods. The Cu^{2+}-labeling assay was less efficient than the assay based on FITC-labeling because of the involvement of a two-step procedure. The initial capping ligand on the Au nanostructures played a key role in determining both the efficiency and kinetics of the ligand exchange process. This study provides a set of useful guidelines for PEGylation of Au nanostructures, as well as for surface modification with other compounds or polymers, in an effort to improve the *in vivo* delivery of nanomaterials.

Methods

Chemicals and materials

Fluorescamine was purchased from Invitrogen (Carlsbad, CA). HS-PEG$_{5000}$-NH$_2$ (M.W. $\approx$ 5,000) and HS-PEG$_{20000}$-NH$_2$ (M.W. $\approx$ 20,000) were purchased from Laysan Bio (Arab, AL), HS-PEG$_{3000}$-NH$_2$ (M.W. $\approx$ 3,000) was obtained from Rapp Polymere GmbH (Tübingen, Germany). 1,4,7,10-Tetraazacyclodocecane-1,4,7,10-tetreaacetic acid mono (N-hydroxysuccinimide ester) (DOTA-NHS, ≥90%) was obtained from Macrocyclics (Dallas, TX). The Kaiser test kit was obtained from Fluka (Buchs, Switzerland). Fluorescein isothiocyanate (FITC, ~98%), Chelex 100 resin (50–100 mesh), copper(II) chloride (CuCl$_2$, ~99.9%), gold(III) chloride trihydrate (HAuCl$_4$·3H$_2$O, ≥99.0%), sodium borohydride (NaBH$_4$, 99%), L-ascorbic acid (>99%), silver nitrate (AgNO$_3$, >99%), poly(vinyl pyrrolidone) (PVP, M.W. $\approx$ 55,000), cetyltrimethylammonium bromide (CTAB, ≥99%), cetyltrimethylammonium chloride (CTAC, ≥98%), and 1,10-phenanthroline ethylenediaminetetraacetic acid (EDTA, ≥99%) were all obtained from Sigma-Aldrich (St. Louis, MO). All the chemical reagents were used as received. Water with a resistivity of 18 MΩ·cm was prepared using a E-Pure filtration system from Barnstead International

(Dubuque, IA). The water and buffer solutions used for Cu^{2+} labeling were treated with Chelex 100 overnight prior to use.

Synthesis of Au Nanostructures

The 30-, 50-, and 60-nm AuNCs covered by PVP were synthesized using a published procedure.[51] The 40-nm AuNPs capped by CTAC were prepared using a recently reported, two-step procedure.[52] Synthesis of the 42-nm AuNPs capped by citrate ions was conducted using the citrate reduction method.[53] The AuNRs capped by CTAB were prepared using the procedure reported by El-Sayed and coworkers.[54]

PEGylation of Au Nanostructures with HS-PEG-NH$_2$

In a typical process, 1.2 mL of a 0.25 mM aqueous HS-PEG-NH$_2$ solution was added to 3 mL of an aqueous suspension of Au nanostructures (1.7 nM), followed by addition of 1.8 mL H$_2$O to a total volume of 6 mL. The final concentration of Au nanostructures and HS-PEG-NH$_2$ were 0.85 nM and 50 µM, respectively. The reaction mixture was vortexed immediately and then incubated at 4 °C overnight, followed by centrifuging at 14,000 rpm for 5 min. The supernatant was carefully collected, and centrifuged two more times to remove the remaining Au nanostructures. The resultant supernatant solution was subjected to the fluorescamine- and ninhydrin-based assays to determine the number of unreacted HS-PEG-NH$_2$ molecules. The HS-PEG-NH$_2$-functionalized Au nanostructures were washed three more times and then used for conjugation with FITC or DOTA-NHS for corresponding measurements.

Quantification of –S-PEG-NH$_2$ Chains on Au Nanostructures Using Fluorescamine-Based Assay

Prior to analysis, a calibration curve was obtained from a series of HS-PEG-NH$_2$ solutions with known concentrations. Briefly, to each 3 mL of HS-PEG-NH$_2$ standard phosphate buffered (PB, pH = 10) solution, 0.25 mL of 2 µM fluorescamine solution in acetone was added. After 15 min, fluorescence spectra ($\lambda_{ex} \approx 390$ nm, $\lambda_{em} \approx 480$ nm) were recorded. The fluorescent intensities at 480 nm for each solution were plotted as a function of the concentration of HS-PEG-NH$_2$ to generate a calibration curve. For sample measurements, 100 µL of the supernatant solution was diluted into 3 mL with the PB buffer and treated using a procedure similar to what was used for the calibration curve. By comparing the fluorescence intensities with the calibration curve and multiplying the dilution factors, we obtained the concentrations of HS-PEG-NH$_2$ in the supernatant solutions. The number of HS-PEG-NH$_2$ on the Au nanostructures was obtained by subtracting the number of HS-PEG-NH$_2$ in the supernatant from the total number of HS-PEGNH$_2$ added into the suspension of Au nanostructures. This number was then converted to the coverage density by taking into account the total number of Au nanostructures and their total surface area. Each data point represents an average of three replicas.

Quantification of –S-PEG-NH$_2$ Chains on Au Nanostructures Using Ninhydrin-Based Assay

All reagents used for the assay were prepared according to the literature.[55–57] Typically, 6% ninhydrin ethanol solution was prepared by dissolving 2.5 g ninhydrin in 50 mL anhydrous ethanol. The KCN pyridine solution and 80% phenol solution in ethanol from the Kaiser test kit were combined at a 1:1 volume ratio to give a KCN/phenol solution. Prior to assay, a calibration curve was obtained from a series of HS-PEG-NH$_2$ standard solutions with known concentrations. Briefly, to each 250 µL of HS-PEG-NH$_2$ standard solutions, 100 µL 6% ninhydrin ethanol solution and 200 µL KCN/phenol solution were added, followed by heating at 100 °C for 4 minutes. After cooling down in an ice bath, 200 µL 60% wt. ethanol in water was added. UV-vis spectra were then recorded. The calibration curve was generated

by plotting the absorbance at 565 nm as a function of the HS-PEG-NH$_2$ concentration. 250 µL samples (the supernatant solution) were treated using same procedure as that was used for standard solutions. The number of overall HS-PEG-NH$_2$ on the Au nanoparticle was calculated as same as the method of fluorescamine-based assay. Each data point represents an average of three replicas.

Quantification of Active –NH$_2$ Groups on Au Nanostructures by Dye-Labeling Assay

To 500 µL Au-S-PEG-NH$_2$ (with a known concentration), 2 µL of 50 mM FITC in dimethyl sulfoxide (DMSO) was added. The reaction mixture was incubated at room temperature for 15 min, followed by five times washing with water. The pellet was re-dispersed in 500 µL water. To the pellet suspension, 2.5 mL of 40 mM KCN aqueous solution and 2.0 mL water was added to dissolve the Au nanoparticles at room temperature for 30 min. After that, fluorescent spectra ($\lambda_{ex} \approx 488$ nm, $\lambda_{em} \approx 520$ nm) were taken from the sample. The concentration of FITC in each sample was calculated by comparing with the calibration curve obtained for free FITC aqueous solution. The number of active –NH$_2$ groups per Au nanoparticle was calculated from the numbers of FITCs and Au nanoparticles. Each data point represents an average of three replicas.

Quantification of Active –NH$_2$ Groups on Au Nanostructures by Cu^{2+}-Labeling Assay

500 µL of 0.4 nM Au-S-PEG-NH$_2$ was washed 3 times with chelexed water and re-suspended in 500 µL chelexed water. Then, 500 µL of 1 mM DOTA-NHS in 0.1 M PB buffer (pH = 7.4) was added. The reaction mixture was incubated at room temperature for 1 h, followed by washing five times with chelexed water. After the final round of centrifugation, 1 mL of 0.1 M NaOAc buffer (pH = 5.5) was added to re-suspend the pellet, followed by the addition of 10 µL CuCl$_2$ aqueous solution (50 mM). After incubation at 37 °C for 1 h, 500 µL of 1 mM EDTA aqueous solution was added to chelate the unbound Cu^{2+} ions for 15 min. The mixture was washed five times with chelexed water to remove the EDTA-Cu^{2+}, resulting in Au-PEG-DOTA-Cu^{2+}. For Cu^{2+} analysis, 5 µL of the sample solution was dissolved in 0.5 mL of concentrated aqua regia and further diluted to 30 mL using 1% HNO$_3$ aqueous solution prior to ICP-MS measurement. The number of active –NH$_2$ groups per Au nanoparticle could be estimated from the ratio of Cu^{2+} ions to Au nanoparticles from ICP-MS analysis. Each data point represents an average of three replicas.

Instrumentation

TEM images of the Au nanostructures were obtained with a Technai G2 Spirit microscope operated at 120 kV (FEI). Fluorescence spectra were recorded using a Cary Eclipse fluorescence spectrophotometer (Varian). UV-vis spectra were taken with a Cary 50 UV-vis spectrophotometer (Varian). The hydrodynamic diameter of the Au nanostructures was measured in deionized water (pH ≈ 6.7) using dynamic light scattering (Malvern, NanoZS) which was equipped with a zeta-potential analyzer. The concentrations of Au, Ag and Cu elements were determined using ICP-MS (Perkin Elmer, Elan DRC II). The concentration of Au element was then converted to the concentration of Au nanostructures once the particle size and morphology had been determined by TEM.

Supplementary Material

Refer to Web version on PubMed Central for supplementary material.

Acknowledgments

References and Notes

1. Cho EC, Glaus C, Chen J, Welch MJ, Xia Y. Inorganic Nanoparticle-Based Contrast Agents for Molecular Imaging. Trends Mol. Med. 2010; 16:561–573. [PubMed: 21074494]

2. Peer D, Karp JM, Hong S, Farokhzad OC, Margalit R, Langer R. Nanocarriers as an Emerging Platform for Cancer Therapy. Nat. Nanotechnol. 2007; 2:751–760. [PubMed: 18654426]

3. Rosi NL, Mirkin CA. Nanoparticles in Biodiagnostics. Chem. Rev. 2005; 105:1547–1562. [PubMed: 15826019]

4. Lal S, Clare SE, Halas NJ. Nanoshell-Enabled Photothermal Cancer Therapy: Impending Clinical Impact. Acc. Chem. Res. 2008; 41:1842–1851. [PubMed: 19053240]

5. Jain PK, Huang X, El-Sayed IH, El-Sayed MA. Noble Metals on the Nanoscale: Optical and Photothermal Properties and Some Applications in Imaging, Sensing, Biology, and Medicine. Acc. Chem. Res. 2008; 41:1578–1586. [PubMed: 18447366]

6. Xia Y, Li W, Cobley CM, Chen J, Xia X, Zhang Q, Yang M, Cho EC, Brown PK. Gold Nanocages: From Synthesis to Theranostic Applications. Acc. Chem. Res. 2011; 44:914–924. [PubMed: 21528889]

7. Murphy CJ, Gole AM, Stone JW, Sisco PN, Alkilany AM, Goldsmith EC, Baxter SC. Gold Nanoparticles in Biology: Beyond Toxicity to Cellular Imaging. Acc. Chem. Res. 2008; 41:1721–1730. [PubMed: 18712884]

8. Tong L, Zhao Y, Huff TB, Hansen MN, Wei A, Cheng J-X. Gold Nanorods Mediate Tumor Cell Death by Compromising Membrane Integrity. Adv. Mater. 2007; 19:3136–3141. [PubMed: 19020672]

9. Duncan B, Kim C, Rotello VM. Gold Nanoparticle Platforms as Drug and Biomacromolecule Delivery Systems. J. Control. Release. 2010; 148:122–127. [PubMed: 20547192]

10. Bardhan R, Lal S, Joshi A, Halas NJ. Theranostic Nanoshells: From Probe Design to Imaging and Treatment of Cancer. Acc. Chem. Res. 2011; 44:936–946. [PubMed: 21612199]

11. Harris, JM., editor. Poly(ethylene glycol) Chemistry: Biotechnical and Biomedical Applications. New York: Plenum Press; 1992.

12. Karakoti AS, Das S, Thevuthasan S, Seal S. PEGylated Inorganic Nanoparticles. Angew. Chem. Int. Ed. 2011; 50:1980–1994.

13. Neoh KG, Kang ET. Functionalization of Inorganic Nanoparticles with Polymers for Stealth Biomedical Applications. Pol. Chem. 2011; 2:747–759.

14. Knop K, Hoogenboom R, Fischer D, Schubert US. Poly(ethylene glycol) in Drug Delivery: Pros and Cons as Well as Potential Alternatives. Angew. Chem. Int. Ed. 2010; 49:6288–6308.

15. Unsworth LD, Sheardown H, Brash JL. End-Thiolated Poly(ethylene glycol) to Gold: Effect of Surface Chain Density. Langmuir. 2005; 21:1036–1041. [PubMed: 15667186]

16. Perrault SD, Walkey C, Jennings T, Fischer HC, Chan WCW. Mediating Tumor Targeting Efficiency of Nanoparticles Through Design. Nano Lett. 2009; 9:1909–1915. [PubMed: 19344179]

17. Pale-Grosdemange C, Simon ES, Prime KL, Whitesides GM. Formation of Self-Assembled Monolayers by Chemisorption of Derivatives of Oligo(ethylene glycol) of Structure HS(CH2)11(OCH2CH2)mOH on Gold. J. Am. Chem. Soc. 1991; 113:12–20.

18. Latham AH, Williams ME. Versatile Routes Toward Functional, Water-soluble Nanoparticles *via* Trifluoroethylester-PEG-thiol Ligands. Langmuir. 2006; 22:4319–4326. [PubMed: 16618182]

19. Hong R, Fischer NO, Emrick T, Rotello VM. Surface PEGylation and Ligand Exchange Chemistry of FePt Nanoparticles for Biological Applications. Chem. Mater. 2005; 17:4617–4621.

20. Love JC, Estroff LA, Kriebel JK, Nuzzo RG, Whitesides GM. Self-Assembled Monolayers of Thiolates on Metals as a Form of Nanotechnology. Chem. Rev. 2005; 105:1103–1170. [PubMed: 15826011]

21. Wuelfing WP, Gross SM, Miles DT, Murray RW. Nanometer Gold Clusters Protected by Surface-Bound Monolayers of Thiolated Poly(ethylene glycol) Polymer Electrolyte. J. Am. Chem. Soc. 1998; 120:12696–12697.

22. Stark GR. Reactions of Cyanate with Functional Groups of Proteins. III. Reactions with Amino and Carboxyl Groups. Biochemistry. 1965; 4:1030–1036. [PubMed: 5839993]

23. Bender ML. Mechanisms of Catalysis of Nucleophilic Reactions of Carboxylic Acid Derivatives. Chem. Rev. 1960; 60:53–113.

24. Udenfriend S, Stein S, Böhlen P, Dairman W, Leimgruber W, Weigele M. Fluorescamine: A Reagent for Assay of Amino Acids, Peptides, Proteins, and Primary Amines in the Picomole Range. Science. 1972; 178:871–872. [PubMed: 5085985]

25. Kaiser E, Colescott RL, Bossinger CD, Cook PI. Color Test for Detection of Free Terminal Amino Groups in the Solid-phase Synthesis of Peptides. Anal. Biochem. 1970; 34:595–598. [PubMed: 5443684]

26. Sarin VK, Kent SBH, Tam JP, Merrifield RB. Quantitative Monitoring of Solid-phase Peptide Synthesis by the Ninhydrin Reaction. Anal. Biochem. 1981; 117:147–157. [PubMed: 7316187]

27. Ramachandran GK, Hopson TJ, Rawlett AM, Nagahara LA, Primak A, Lindsay SM. A Bond-Fluctuation Mechanism for Stochastic Switching in Wired Molecules. Science. 2003; 300:1413–1416. [PubMed: 12775835]

28. Kamenetska M, Koentopp M, Whalley AC, Park YS, Steigerwald ML, Nuckolls C, Hybertsen MS, Venkataraman L. Formation and Evolution of Single-Molecule Junctions. Phys. Rev. Lett. 2009; 102:126803. [PubMed: 19392306]

29. Frei M, Aradhya SV, Koentopp M, Hybertsen MS, Venkataraman L. Mechanics and Chemistry: Single Molecule Bond Rupture Forces Correlate with Molecular Backbone Structure. Nano. Lett. 2011; 11:1518–1523. [PubMed: 21366230]

30. Aina V, Marchis T, Laurenti E, Diana E, Lusvardi G, Malavasi G, Menabue L, Cerrato G, Morterra C. Functionalization of Sol Gel Bioactive Glasses Carrying Au Nanoparticles : Selective Au Affinity for Amino and Thiol Ligand Groups. Langmuir. 2010; 26:18600–18605. [PubMed: 21090664]

31. Yang ZH, Galloway JA, Yu H. Protein Interactions with Poly(ethylene glycol) Self-Assembled Monolayers on Glass Substrates: Diffusion and Adsorption. Langmuir. 1999; 15:8405–8411.

32. Tsukanova V, Salesse C. On the Nature of Conformational Transition in Poly(ethylene glycol) Chains Grafted onto Phospholipid Monolayers. J. Phys. Chem. B. 2004; 108:10754–10764.

33. Wanwimolruk S, Birkett DJ, Brooks PM. Structural Requirements for Drug Binding to Site II on Human Serum Albumin. Mol. Pharmacol. 1983; 24:458–463. [PubMed: 6195516]

34. Matsuura H, Fukuhara K. Conformational Analysis of Poly(oxyethylene) Chain in Aqueous Solution as a Hydrophilic Moiety of Nonionic Surfactants. J. Mol. Struct. 1985; 126:251–260.

35. Yoshihara T, Tadokoro H, Murahashi S. Normal Vibrations of the Polymer Molecules of Helical Conformations. IV. Polyethylene Oxide and Polyethylene-d_4 Oxide. J. Chem. Phys. 1964; 41:2902–2911.

36. Ahmad B, Ansari MA, Sen P, Khan RH. Low versus High Molecular Weight Poly(ethylene glycol)-Induced States of Stem Bromelain at Low pH: Stabilization of Molten Globule and Unfolded States. Biopolymers. 2006; 81:350–359. [PubMed: 16345002]

37. Chaput SB, Carrot C. Interactions of Active Carbon with Low- and High-Molecular Weight Polyethylene Glycol and Polyethylene Oxide. J. App. Polym. Sci. 2006; 100:3490–3497.

38. Sokolov K, Chumanov G, Cotton TM. Enhancement of Molecular Fluorescence near the Surface of Colloidal Metal Films. Anal. Chem. 1998; 70:3898–3905. [PubMed: 9751028]

39. Geddes CD, Lakowicz JR. Editorial: Metal-Enhanced Fluorescence. J. Fluorescence. 2002; 12:121–129.

40. Xia X, Yang M, Oetjen LK, Zhang Y, Li Q, Chen J, Xia Y. An Enzyme-Sensitive Probe for Photoacoustic Imaging and Fluorescence Detection of Protease Activity. Nanoscale. 2011; 3:950–953. [PubMed: 21225037]

41. Yun CS, Javier A, Jennings T, Fisher M, Hira S, Peterson S, Hopkins B, Reich NO, Strouse GF. Nanometal Surface Energy Transfer in Optical Rulers, Breaking the FRET Barrier. J. Am. Chem. Soc. 2005; 127:3115–3119. [PubMed: 15740151]

42. Li WP, Meyer LA, Capretto DA, Sherman CD, Anderson CJ. Receptor Binding, Biodistribution, and Metabolism Studies of ^{64}Cu-DOTA-Cetuximab, a PET Imaging Agent for Epidermal Growth-factor Receptor-positive Tumors. Cancer Biother. Radiopharm. 2008; 23:158–171. [PubMed: 18454685]

43. Eiblmaier M, Meyer LA, Watson MA, Fracasso PM, Pike LJ, Anderson CJ. Correlating EGFR Expression with Receptor-Binding Properties and Internalization of ^{64}Cu-DOTA-Cetuximab in 5 Cervical Cancer Cell Lines. J. Nucl. Med. 2008; 49:1472–1479. [PubMed: 18703609]

44. Jarrett BR, Gustafsson B, Kukis DL, Louie AY. Synthesis of ^{64}Cu-labeled Magnetic Nanoparticles for Multimodal Imaging. Bioconjug. Chem. 2008; 19:1496–1504. [PubMed: 18578485]

45. Levin CS, Bishnoi SW, Grady NK, Halas NJ. Determining the Conformation of Thiolated Poly(ethylene glycol) on Au Nanoshells by Surface-Enhanced Raman Scattering Spectroscopic Assay. Anal. Chem. 2006; 78:3277–3281. [PubMed: 16689527]

46. Weisbecker CS, Merritt MV, Whitesides GM. Molecular Self-Assembly of Aliphatic Thiols on Gold Colloids. Langmuir. 1996; 12:3763–3772.

47. Hostetler MJ, Templeton AC, Murray RW. Dynamics of Place-Exchange Reactions on Monolayer-Protected Gold Cluster Molecules. Langmuir. 1999; 15:3782–3789.

48. Nikoobakht B, El-Sayed MA. Evidence for Bilayer Assembly of Cationic Surfactants on the Surface of Gold Nanorods. Langmuir. 2001; 17:6368–6374.

49. Gole A, Murphy CJ. Polyelectrolyte-Coated Gold Nanorods: Synthesis, Characterization and Immobilization. Chem. Mater. 2005; 17:1325–1330.

50. Yu CX, Varghese L, Irudayaraj J. Surface Modification of Cetyltrimethylammonium Bromide-Capped Gold Nanorods to Make Molecular Probe. Langmuir. 2007; 23:9114–9119. [PubMed: 17636999]

51. Skrabalak SE, Au L, Li X, Xia Y. Facile Synthesis of Ag Nanocubes and Au Nanocages. Nat. Protoc. 2007; 2:2182–2190. [PubMed: 17853874]

52. Ma Y, Li W, Cho EC, Li Z, Yu T, Zeng J, Xie Z, Xia Y. Au@Ag Core-Shell Nanocubes with Finely Tuned and Well-Controlled Sizes, Shell Thicknesses, and Optical Properties. ACS Nano. 2010; 4:6725–6734. [PubMed: 20964400]

53. Frens G. Controlled Nucleation for the Regulation of the Particle Sice in Monodisperse Gold Suspensions. Nature. 1973; 241:20–22.

54. Nikoobakht B, El-Sayed MA. Preparation and Growth Mechanism of Gold Nanorods (NRs) Using Seed-Mediated Growth Method. Chem. Mater. 2003; 15:1957–1962.

55. Curotto E, Aros F. Quantitative Determination of Chitosan and the Percentage of Free Amino Groups. Anal. Biochem. 1993; 211:240–241. [PubMed: 8317699]

56. Moore SJ. Amino Acid Analysis: Aqueous Dimethyl Sulfoxide Solvent for the Ninhydrin Reaction. J. Biol. Chem. 1968; 243:6281–6283. [PubMed: 5723468]

57. Sheng SJ, Kraft JJ, Schuster SM. A Specific Quantitative Colorimetric Assay for L-Asparagine. Anal. Biochem. 1993; 221:242–249. [PubMed: 8100404]
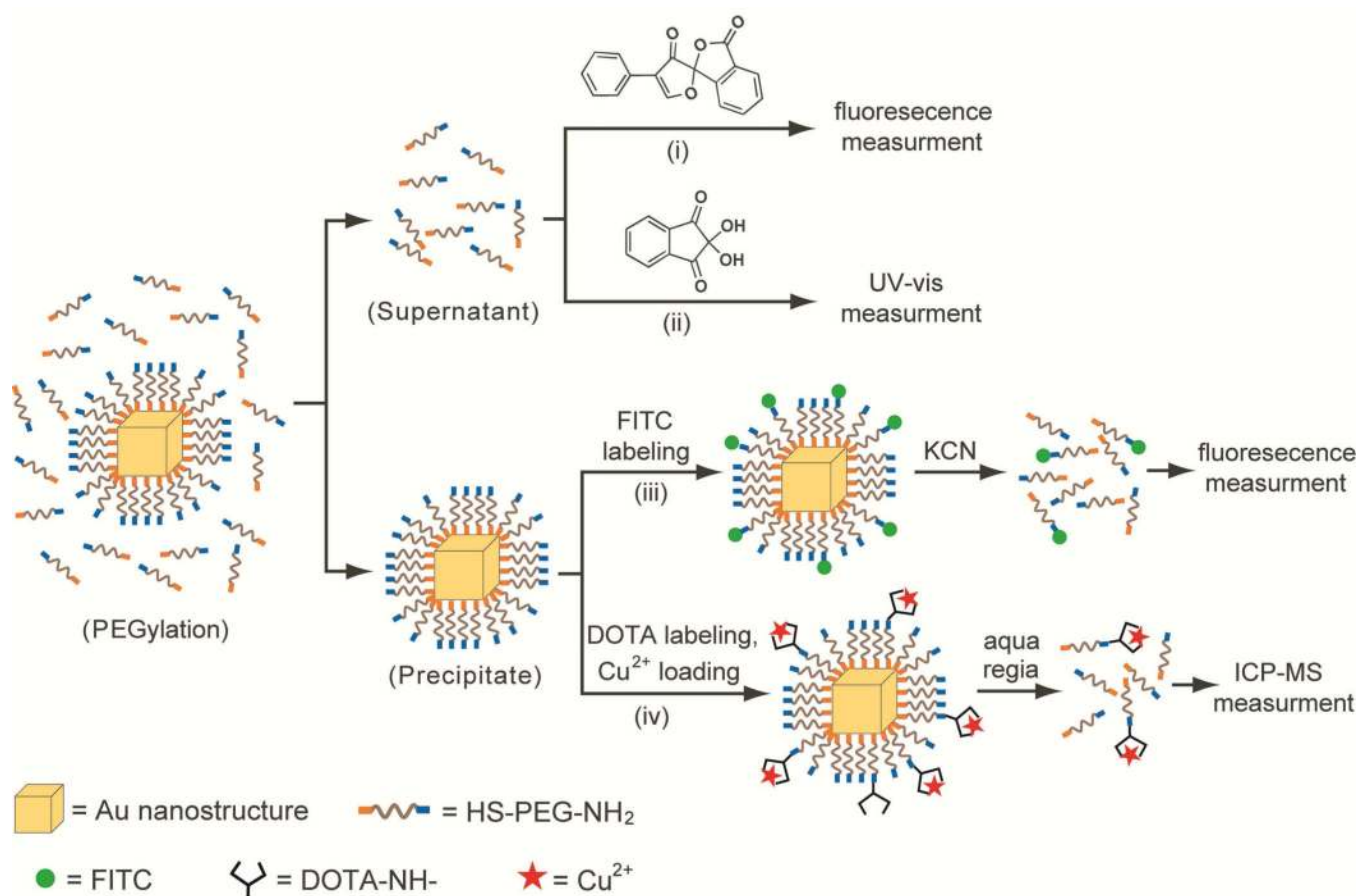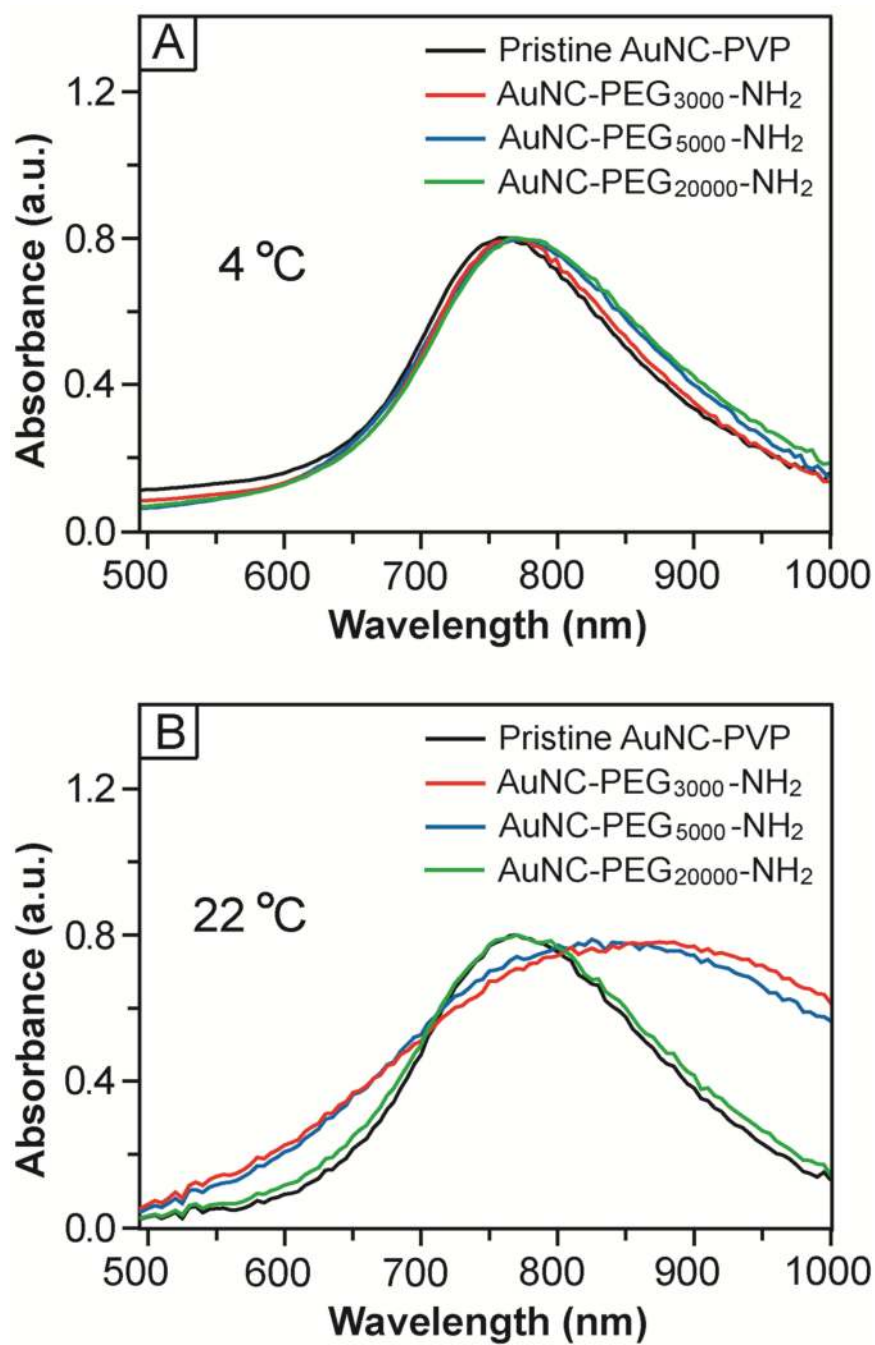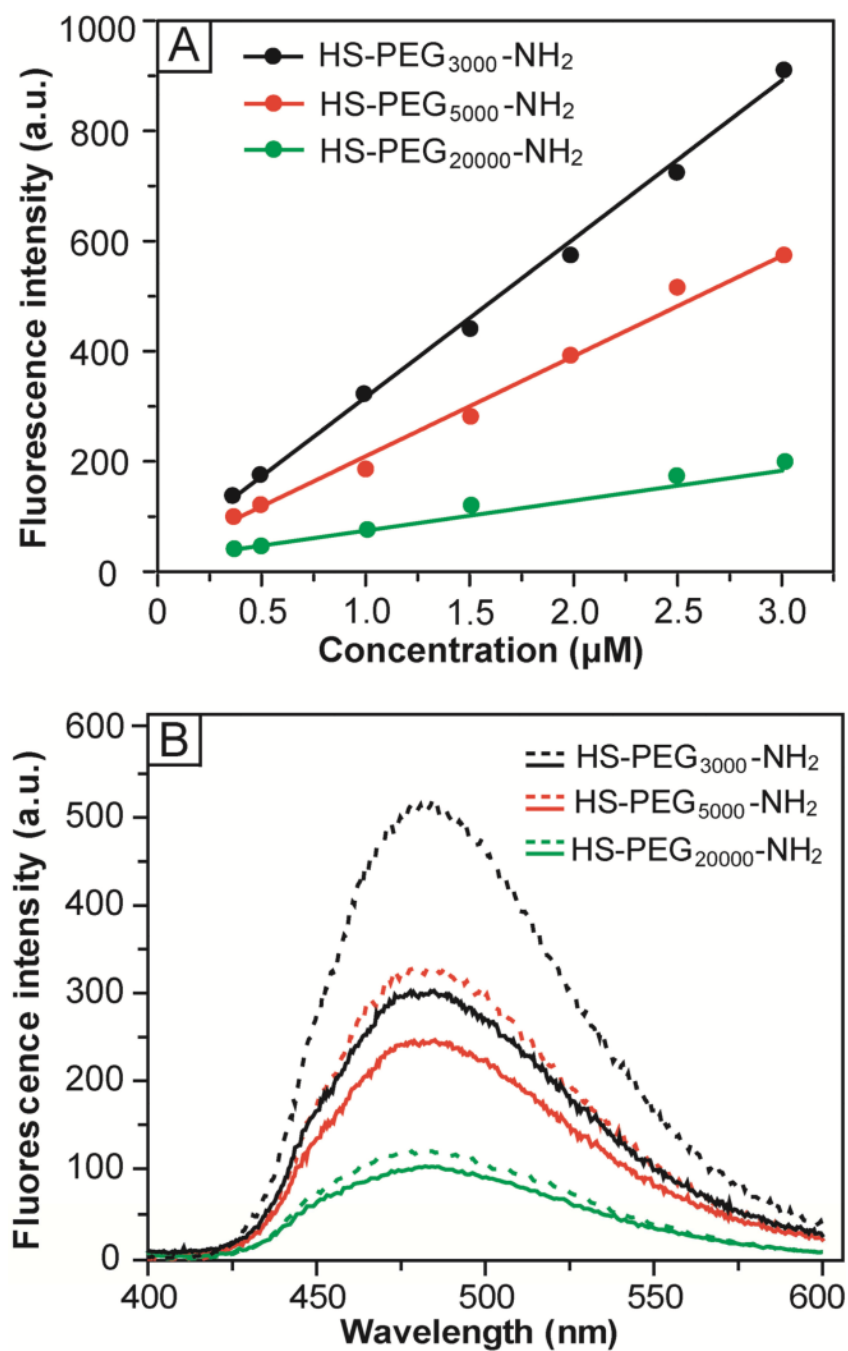
Figure 1.
Schematic illustration of the four methods for quantifying the average number of –S-PEG-NH_2 chains on the surface of one single Au nanostructure: *i*) fluorescamine-based assay, *ii*) ninhydrin-based assay, *iii*) FITC-labeling assay, and *iv*) Cu^{2+}-labeling assay.
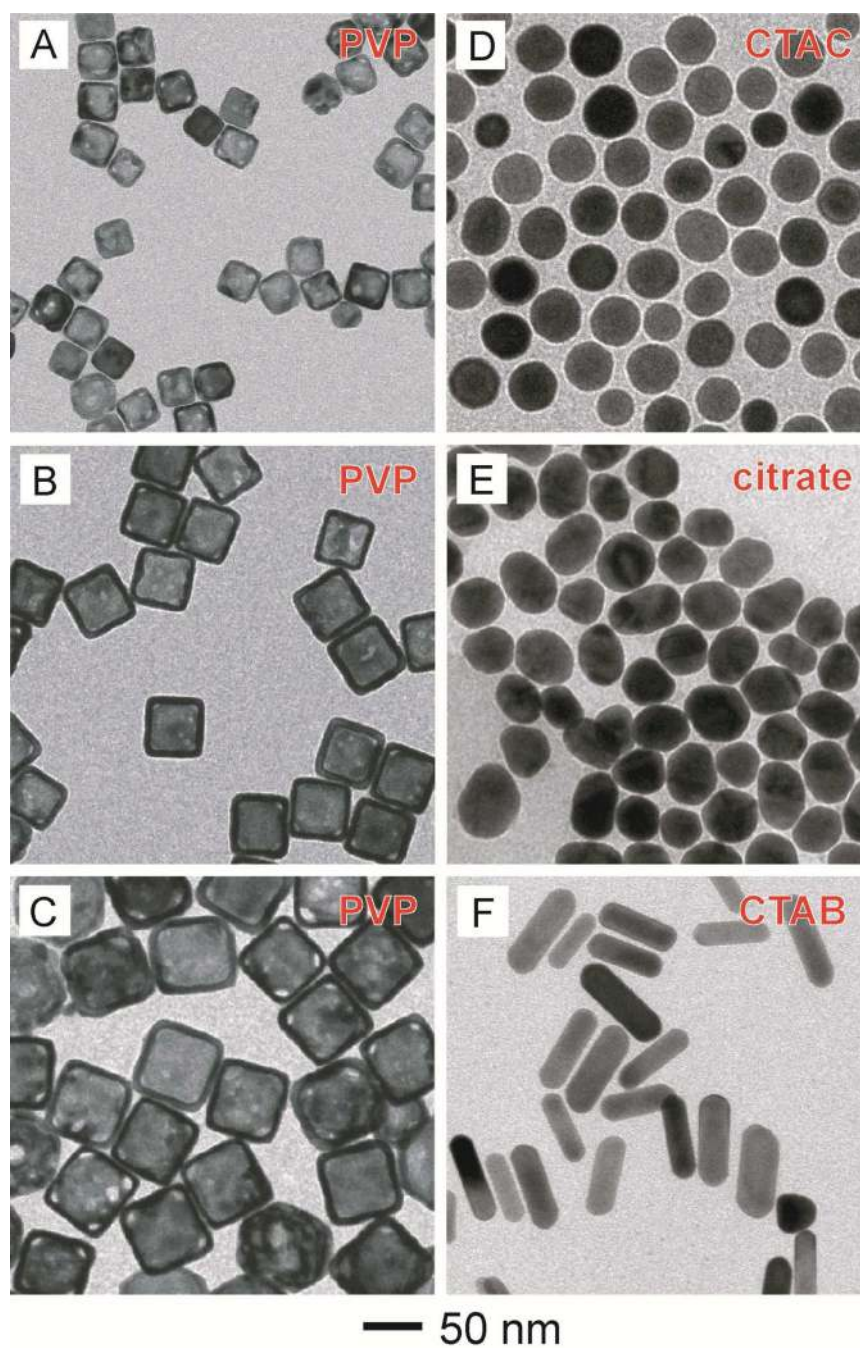
Figure 2.
TEM images of the different types of Au nanostructures used in this work: (A–C) PVP-capped AuNCs with average edge lengths of 30, 50, and 60 nm, respectively, (D) CTAC-capped AuNPs with an avarage diameter of 40 nm, (E) citrate-capped AuNPs with an avarage diameter of 42 nm, and (F) CTAB-capped AuNRs with avarage dimensions of 80 nm × 22 nm.
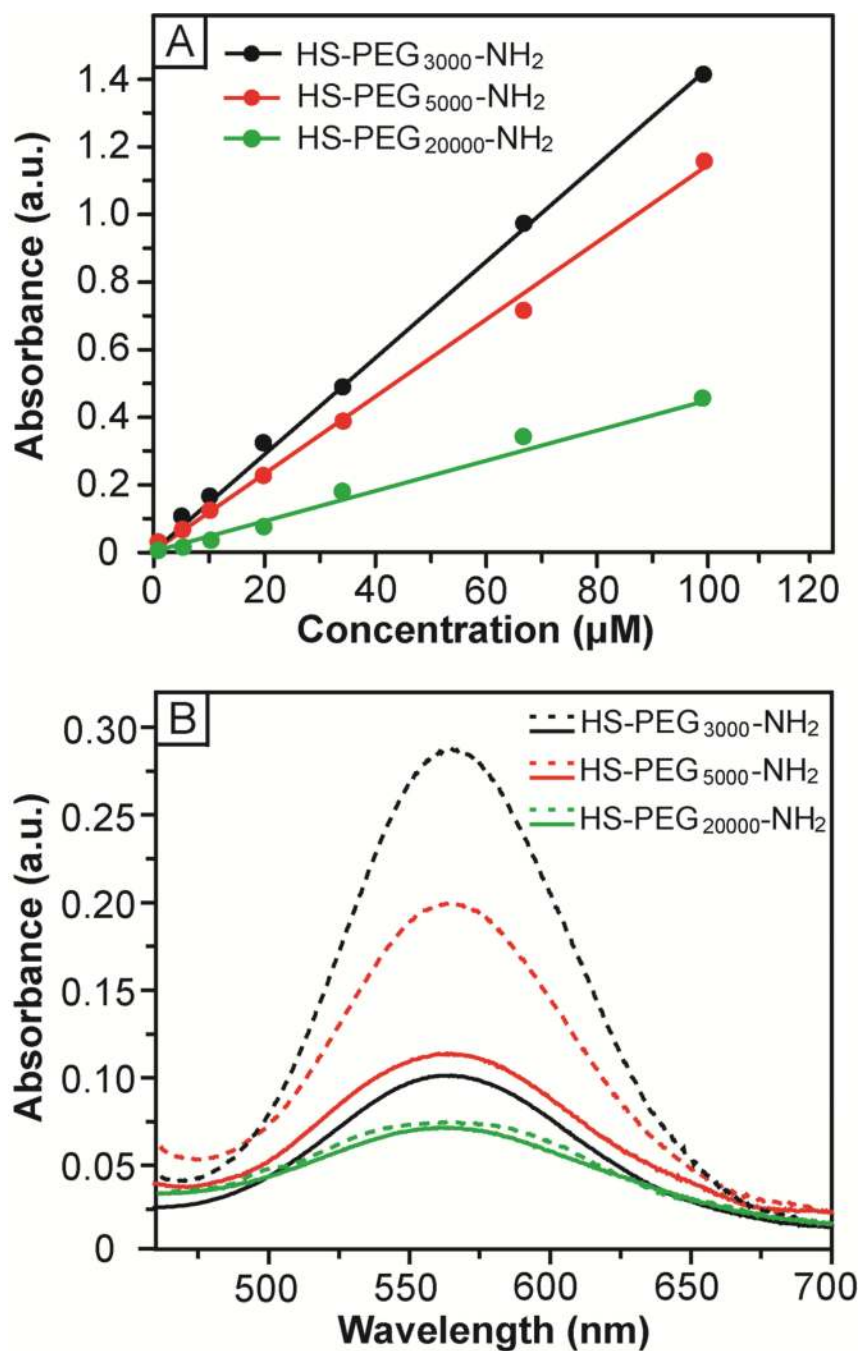
Figure 3.
UV-vis spectra of 50-nm AuNCs before and after functionalization with HS-PEG-NH_2 at two different temperatures: (A) 4 °C and (B) 22 °C. Note that the AuNCs showed significant broadening for their peaks due to aggregation when they were functionalized with HS-PEG_{3000}-NH_2 or HS-PEG_{5000}-NH_2 at 22 °C.
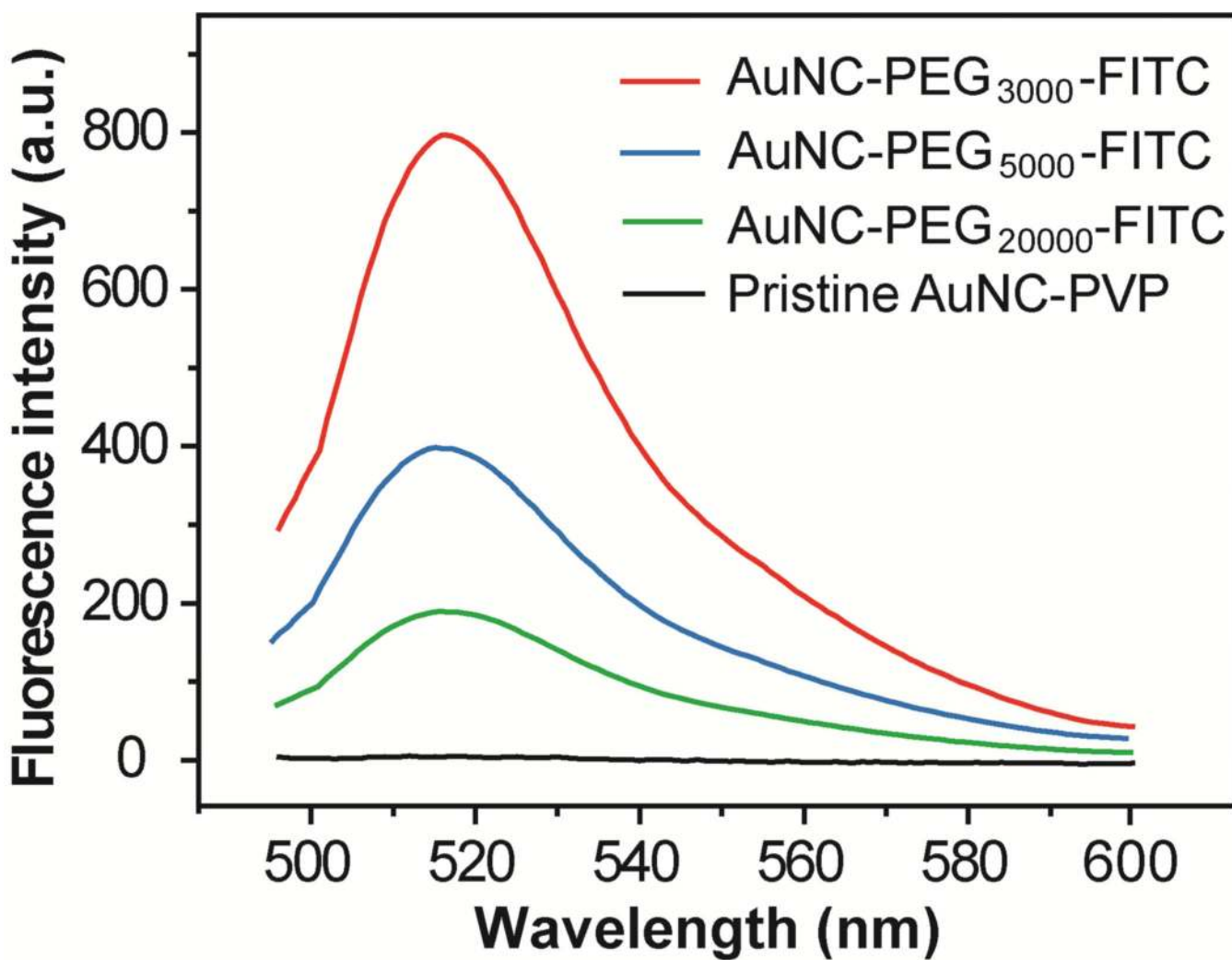
Figure 4.
(A) Calibration curves for HS-PEG-NH$_2$ and fluorescamine-based assay at pH = 10, showing a linear relationship between the fluorescence intensity at 480 nm and the concentration of HS-PEG-NH$_2$. (B) Fluorescence spectra corresponding to the chromophore derived from a reaction between fluorescamine and HS-PEG$_{3000}$-NH$_2$ (black curves), HS-PEG$_{5000}$-NH$_2$ (red curves), and HS-PEG$_{20000}$-NH$_2$ (green curves), respectively. The doted and solid curves correspond to the spectra taken from the original solution and the supernatant after incubation with 50-nm AuNCs for 12 h, respectively.
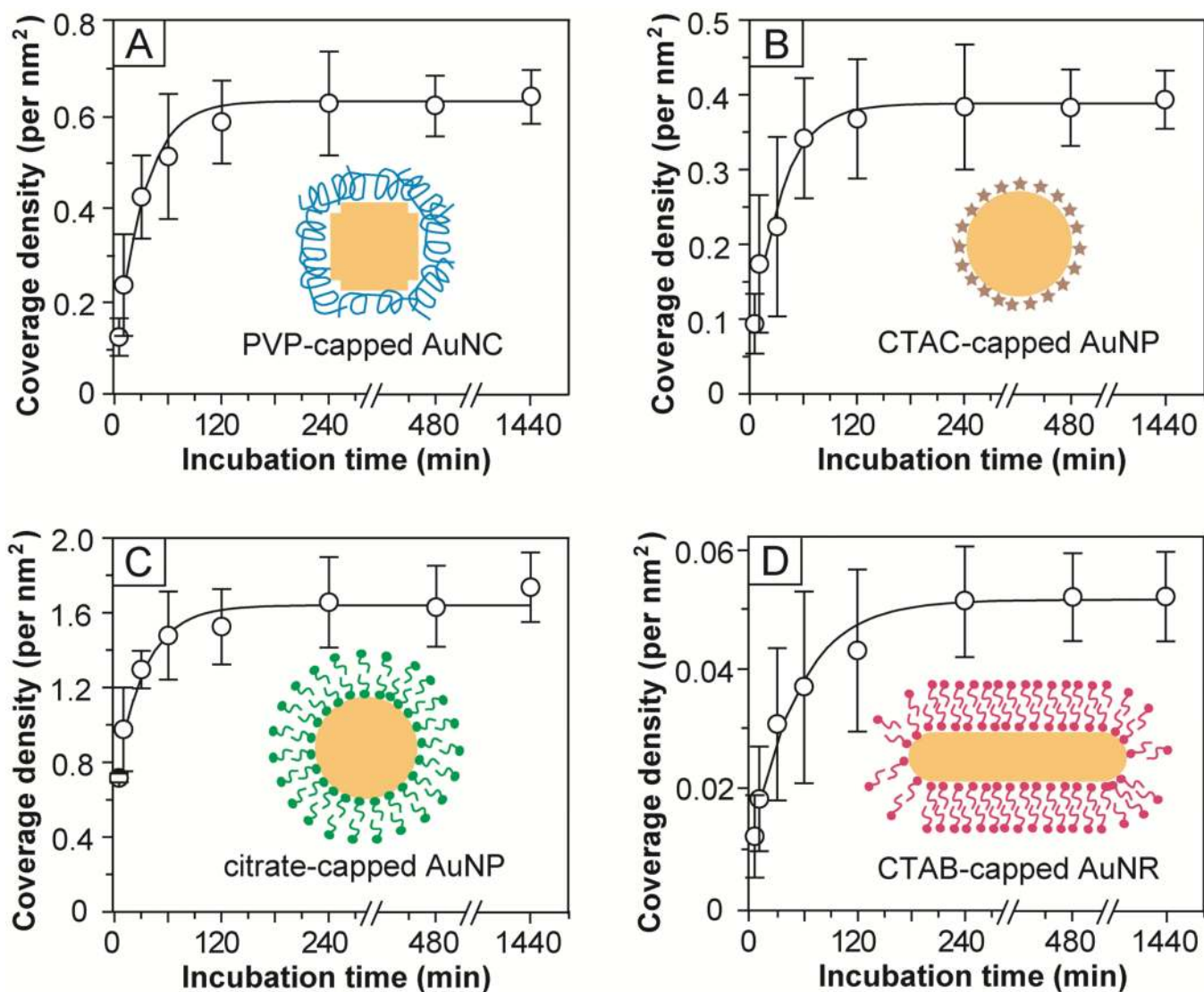
Figure 5.
(A) Calibration curves for HS-PEG-NH$_2$ and ninhydrin-based assay, showing a linear relationship between the absorbance at 565 nm and the concentration of HS-PEG-NH$_2$. (B) UV-vis spectra of the chromophore derived from a reaction between ninhydrin and HS-PEG$_{3000}$-NH$_2$ (black curves), HS-PEG$_{5000}$-NH$_2$ (red curves), and HS-PEG$_{20000}$-NH$_2$ (green curves), respectively. The dotted and solid curves correspond to spectra taken from the original solution and from the supernatant after incubation with 50-nm AuNCs for 12 h, respectively.

Figure 6.
Fluorescence spectra of the solutions containing AuNC-S-PEG-FITC after the AuNCs had been dissolved with a KCN-based etchant: AuNC-S-PEG$_{3000}$-FITC (10 pM, red curve), AuNC-S-PEG$_{5000}$-FITC (10 pM, blue curve), AuNC-S-PEG$_{20000}$-FITC (20 pM, green curve) and the pristine AuNC (20 pM, black curve).

Figure 7.
Adsorption kinetics for the PEGylation of various types of Au nanostructures with HS-PEG$_{5000}$-NH$_2$ as measured by the fluorescamine-based assay. The error bars represent standard deviation from six replicas for each measurement. The inset depicts the morphology of each type of Au nanostructure and its surface capping layer.

Table 1

Characterization of the AuNCs before and after functionalization with HS-PEG-NH$_2$.[a]

HS-PEG-NH$_2$ (Dalton)	Hydrodynamic diameter (nm)	Zeta potential (mV)	Total PEGs per AuNC[b]	Total PEGs per AuNC[c]	Active PEGs per AuNC[d]	Active PEGs per AuNC[e]
no PEG	96.1	−47.9	—	—	—	—
3,000	108.1	20.3	24,700±1,200	33,170±2,750	8,860±990	7,000±3,200
5,000	130.1	11.7	12,700±3,340	20,000±2,400	4,760±870	3,800±2,100
20,000	113.9	−35	2,100±740	3,200±1,770	1,010±620	760±400

[a]The edge length of the AuNCs was measured to be 50 nm by TEM

[b]Measured by the fluorescamine-based assay

[c]Measured by the ninhydrin-based assay

[d]Measured by the FITC-labeling assay

[e]Measured by the Cu^{2+}-labeling assay

Table 2

The coverage densities of –S-PEG-NH$_2$ chains on various types of Au nanostructures.[a]

Gold nanostructures	Coverage density of PEG-NH$_2$ chains[b]	Coverage density of active -NH$_2$ groups[c]
PVP-capped AuNCs[d]	0.61	0.19
CTAC-capped AuNPs	0.41	0.22
citrate-capped AuNPs	1.63	1.01
CTAB-capped AuNRs	0.052	0.029

[a] The coverage density is defined as the number of PEG-NH$_2$ chains per nm^2 of Au surface

[b] Measured by the fluorescamine-based assay

[c] Measured by the FITC-labeling assay

[d] The inner surface and pores of the AuNCs were not included